Giant Kohn Anomaly and the Phase Transition in Charge Density Wave $ZrTe_3$

Moritz Hoesch,[1] Alexey Bosak,[1] Dmitry Chernyshov,[2] Helmuth Berger,[3] and Michael Krisch[1]

[1]*European Synchrotron Radiation Facility, 6 rue Jules Horowitz, 38043 Grenoble Cedex, France*

[2]*Swiss-Norwegian Beam Lines at the ESRF, 6 rue Jules Horowitz, 38043 Grenoble Cedex, France*

[3]*Ecole Polytechnique Federale de Lausanne, Institut de Physique de la Matiere Complexe, 1015 Lausanne, Switzerland*

(Received 28 November 2008; published 25 February 2009)

A strong Kohn anomaly in $ZrTe_3$ is identified in the mostly transverse acoustic phonon branch along the modulation vector q_P with polarization along the a^* direction. This soft mode freezes to zero frequency at the transition temperature T_P, and the temperature dependence of the frequency is strongly affected by fluctuation effects. Diffuse x-ray scattering of the incommensurate superstructure shows a power-law scaling of the intensity and the correlation length that is compatible with an order parameter of dimension $n = 2$.

DOI: 10.1103/PhysRevLett.102.086402 PACS numbers: 71.45.Lr, 63.20.kd, 71.30.+h

Dynamical modulations of the spin or charge density are a ubiquitous phenomenon in crystalline metals and form an important ingredient in solid state theory [1]. In many materials, they remain dynamical at all temperatures and contribute to the rich phenomenology of electronic, magnetic, and thermal transport and ordering. Recently, their role has been rediscussed in high T_c superconducting and colossal magnetoresistance oxides, in connection with the formation of striped charge order [2]. Similar to the stripes, a static charge density wave (CDW) removes spectral weight from the Fermi level, while the superconductivity can be supported by dynamical density waves. In general, the modulation wave vector $\vec{q}$ can be incommensurate with the underlying lattice and is derived from a nesting geometry of the Fermi surface that provides strong screening at $\vec{q} = 2\vec{k}_F$. Such a nested Fermi surface is found, in particular, in low-dimensional crystal structures with chainlike atomic arrangements [1].

Because of the low-dimensional nature, the phase transition, the so-called Peierls transition, to the statically modulated ground state of the one-dimensional chain is strongly affected by fluctuations [3]. Inelastic neutron scattering studies revealed a giant Kohn anomaly in KCP [4] and blue bronze [5], whereas $(TaSe_4)_2I$ [6,7] displayed a temperature-dependent soft mode, which did, however, not attain zero frequency at the Peierls transition temperature T_P. An inelastic x-ray scattering study of the prototypical 1D compound $NbSe_3$ failed to show any clear Kohn anomaly but only a broadening of an acoustic phonon mode at the first modulation vector $\vec{q}_1$ of $NbSe_3$ [8].

The modulated ground state itself is readily observed by the appearance of new diffraction peaks, with a position in the reciprocal lattice that represents the modulation vector $\vec{q}$. Similar to other structural phase transitions, the temperature dependence of these superstructure reflections is used to study the ordering of the CDW modulation. Again, only a small number of 1D inorganic chain systems show this transition, and very few studies exist. These find that the Peierls transition is governed by a critical exponent of the order parameter, which is compatible with an order parameter of dimension $n = 2$ [blue bronze [9]] or close to being a (blurred) first-order transition [$(TaSe_4)_2I$ [10]]. A clear assignment to a particular universality class has, however, not been found, and the question remains open whether the transition can be classified in this way.

While the CDW ground state and its many fascinating properties are well described by theory [1], the phase transition is accessible only by experiment. In this Letter, we present an experimental study of the fluctuations and the soft-mode phonon in $ZrTe_3$ to elucidate the properties of the charge density wave in the important regime close to and above the phase transition, where the density waves are of dynamical nature.

$ZrTe_3$ crystallizes in a monoclinic structure with space group $P2_1/m$ (lattice parameters $a = 5.89$ Å, $b = 3.93$ Å, $c = 10.09$ Å, $\alpha = \gamma = 90°$, and $\beta = 97.8°$). $(ZrTe_3)_\infty$ chains similar to $NbSe_3$ run along b. Only one type of chain is present in the unit cell. The Peierls modulation $\vec{q}_P = (0.07, 0, 0.333)$ (reciprocal lattice units) [11] is transverse to these prismatic chains with a small a^* component and a tripling of the unit cell along the layering c^* direction. The modulation is thus very different from $NbSe_3$ and mostly in the almost equidistant Te-Te chains along a, where the prismatic chains are laterally bonded. Resistivity measurements show an anomaly due to the transition at $T_P = 63$ K, and the system remains metallic below T_P [12]. Electronic structure calculations [13,14] and a detailed photoemission study [15] explain this behavior by nesting in a small electron pocket of the highly directional Te $5p_x$ band running along these Te-Te chains, while other sheets of the Fermi surface remain unaffected by the transition. The opening of a gap in the electronic dispersion of this band was found to follow a BCS model of the Peierls transition with a mean field transition temperature T_{MF} about 4 times higher than T_P [15]. Last, but not least, the phase transition gives rise to a very small specific heat anomaly at T_P [16].

The experiment was performed at the inelastic x-ray scattering (IXS) beam line ID28 at the European Synchrotron Radiation Facility. Phonon dispersions were measured with an energy resolution $\delta E = 1.7$ meV. The momentum resolution was $\delta Q = 0.05$ Å^{-1} in the horizontal $a^* - b^*$ plane and 0.15 Å^{-1} in the vertical c^* direction. Diffuse scattering and diffraction scans were recorded with an energy-integrating detector at the same wavelength of $\lambda = 0.57$ Å and similar momentum resolution. The samples were grown by chemical vapor transport and formed platelets of $1 \times 2 \times 0.1$ mm^3 along a, b, and c, respectively, that were glued to the copper cold finger of a closed cycle cryostat using silver paste. The absolute temperature scale was calibrated relative to a diode thermometer mounted on the cold finger by setting the inflection point of the intensity of critical scattering at T_P to the known $T_P = 63$ K (see Fig. 4).

The phonon dispersion along the CDW modulation vector was determined as shown in Fig. 1. IXS spectra were recorded for each momentum transfer $\vec{Q}$ close to the strong Bragg spot $\vec{G} = (40\bar{1})$, along a straight line from $(40\bar{1})$ through $\vec{q}_P$ and beyond, as shown in the inset in Fig. 1. In the figure, the a^* component of $\vec{Q}$ is indicated in relative lattice units. At a temperature $T = 100$ K $= 1.6T_P$, the spectra are dominated by a central peak at zero energy loss for all momenta, in particular, close to $\vec{q}_P$ ($a^* = 3.93$) and on approaching the Γ point (lowest curve). The spectra are fit by a sum of three or five terms for one or two phonons, respectively. The first term is the central peak, and the following terms are phonons in Stokes and anti-Stokes positions with their intensity ratio given by the detailed balance at the corresponding temperature. No convolution was performed, and the model function was a sum of shifted resolution functions according to these terms, thereby assuming that broadening effects will be small with respect to the experimental resolution, as they cannot be resolved in the strongly overlapping peaks. This method yielded smooth and self-consistent phonon dispersions.

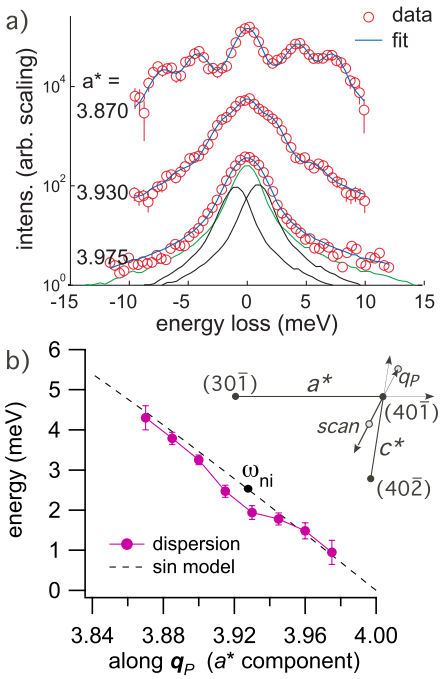

FIG. 1 (color online). Acoustic phonon along $\vec{q}_P$ at $T = 100$ K. (a) Representative IXS spectra at momenta close to $(40\bar{1})$ at $\vec{q}_P$ ($a^* = 3.93$) and across $\vec{q}_P$ on a logarithmic scale with arbitrary offset. Error bars are smaller than the symbols except for the outer data points. Solid lines below that data are (shifted) resolution functions that were summed to fit the data. (b) Phonon dispersion extracted from fits to the IXS data. The dashed line is a sinusoidal model dispersion $\omega_{ni}(\vec{q})$ that serves as a guide to the eye. The inset shows a portion of reciprocal space with the scan direction through $\vec{q}_P$ indicated.

The thus extracted dispersion is displayed in Fig. 1(b). It shows a dip at $\vec{q}_P$ deviating from a sinusoidal model dispersion. This Kohn anomaly is a direct manifestation of the Fermi surface nesting vector $2k_F$. No such anomaly was observed for other acoustic phonons; in particular, a scan along the high symmetry direction a^* (longitudinal acoustic phonon) did not show any anomaly, although the Fermi surface could also afford a certain nesting along this direction. All other modes that were studied did not show any anomalies, and also a Raman scattering study of the phonon modes at the Γ point did not show any anomalous temperature dependence [17]. The line along $\vec{q}_P$ corresponds to an almost transverse dispersion along the large c^* component. The phonon polarization is along a^*. Thus, the displacement pattern of the soft mode is of mostly transverse character with respect to the Te-Te chains whose Te $5p_x$ orbitals form the quasi-one-dimensional Fermi surface.

The temperature dependence of the Kohn anomaly is traced in Fig. 2. As mentioned above, already at room temperature ($4.6T_P$) a slight dip is visible, barely outside the experimental error bars. As the temperature is lowered, the dip gets more pronounced, until the phonon frequency drops rapidly to zero at T_P. Mean field theory predicts this freezing of the phonon as a logarithmic divergence that would correspond to a square-root power law close to the phase transition [1]. Inspection of our data by plotting on a double-logarithmic scale did not reveal a well-defined power-law behavior. Over a broad range in temperature, the closest correspondence to a power law was approximately $(T - T_P)^{1/8}$. On the linear scale in Fig. 2, this $1/8$ power law and the theoretical expectation of a $1/2$ power law are shown. Thus, we conclude that the soft mode freezes in the fashion of a giant Kohn anomaly. Our results suggest that the phonon frequency drops to zero at the phase transition. Above the transition, fluctuation effects lead to a much more rapid recovery of the noninteracting phonon frequency than the logarithmic dependence predicted by mean field theory.

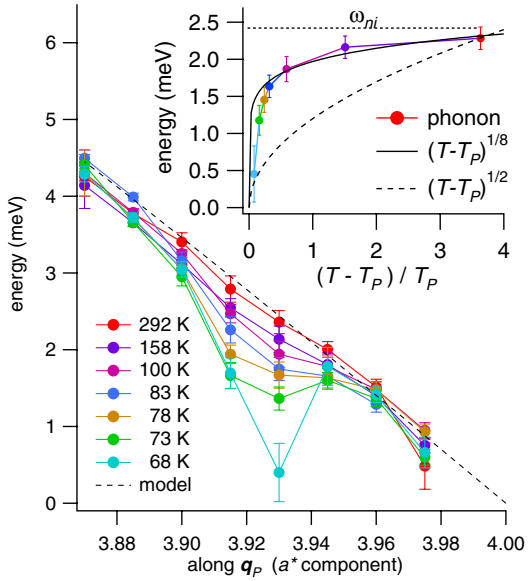

FIG. 2 (color online). Phonon dispersion from $(40\bar{1})$ in the direction of $\vec{q}_P$ at various temperatures $T > T_P$ above the transition. The inset shows the phonon energy $\hbar\omega_q$ at $\vec{q}_P$ as a function of reduced temperature $(T - T_P)/T_P$. The solid and dashed lines represent a $1/8$ and a $1/2$ power law, respectively.

The deviation from mean field behavior led us to investigate the thermodynamic signature of the phase transition by the study of the diffuse scattering ($T > T_P$) and superstructure intensity ($T < T_P$) at $\vec{q}_P$. Again, the experimental difficulty lies in the close proximity to the Bragg reflection due to the small component a^* of $\vec{q}_P$. A survey of momentum space slightly above T_P showed that the diffuse scattering signal is present for $\vec{Q} = \vec{G} \pm \vec{q}_P$ when $\vec{G}$ has a strong component along the a^* direction of the reciprocal lattice.

Our combined diffuse and inelastic x-ray scattering study allows disentangling the static and dynamical contributions to the diffuse intensity. On inspection, the IXS spectra show that the dominant contribution is the central peak (zero energy loss). Figure 3(a) compares the intensity of the central peak and the phonon (symbols) with the energy integrated signal (line) at $T = 73\ \mathrm{K} > T_P$. The central peak is not only dominant, but its momentum dependence corresponds to that of the diffuse scattering signal. Thus we can interpret the diffuse scattering as a quasistatic diffraction feature which is representative of the (fluctuating) order of the CDW.

Scans of the integrated scattering intensity along $\vec{q}_P$ are displayed in Fig. 3(b) and show the emergence of a diffuse scattering feature. Because of the strong background of thermal diffuse scattering (TDS) from the acoustic phonon (dominating at high temperatures), the peak shape is not easily determined. A reliable measurement, however, is possible for scans through $\vec{q}_P$ along b^* as the rocking curve along this direction is sharp and no resolution broadening affects the width of the intensity profiles. Again, at high temperature a broad peak is partially due to TDS, but the emergence of a sharp feature with decreasing width at lower T is due to the longer correlation length of the CDW order. Below T_P, this peak does not sharpen any further, although it remains slightly broadened with respect to the experimental resolution. Its intensity grows rapidly on lowering the temperature below T_P.

The temperature evolution of the intensity and the width along b^* are shown in Fig. 4. The transition appears slightly broadened around T_P. Outside of this range, the intensity and width show power-law scaling with reduced temperature. The critical exponents derived from these are $2\beta = 0.26 \pm 0.06$ for the intensity, that is taken here as a measure of the order parameter squared, and $\nu = 0.85 \pm 0.2$ for the width, that is proportional to the inverse correlation length. The diffuse scattering peaks as well as the diffraction profiles below T_P were always well represented by a single Lorentzian function. Other critical exponents could

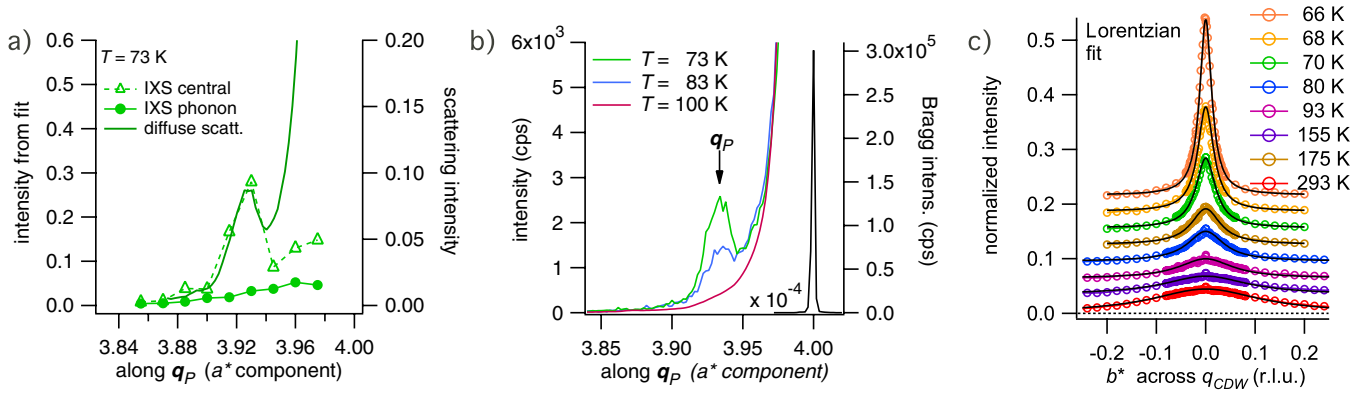

FIG. 3 (color online). Diffuse scattering along $\vec{q}_P$. (a) Symbols represent the intensities extracted from data fitting of the IXS spectra: central peak (triangles), phonon contribution (filled circles). The solid line is the total diffuse scattering intensity as measured with an energy-integrating detector. (b) Diffuse scattering intensities at three selected temperatures as indicated. (c) Scans of diffuse scattering across $\vec{q}_P$ along b^* at various temperatures above T_P.

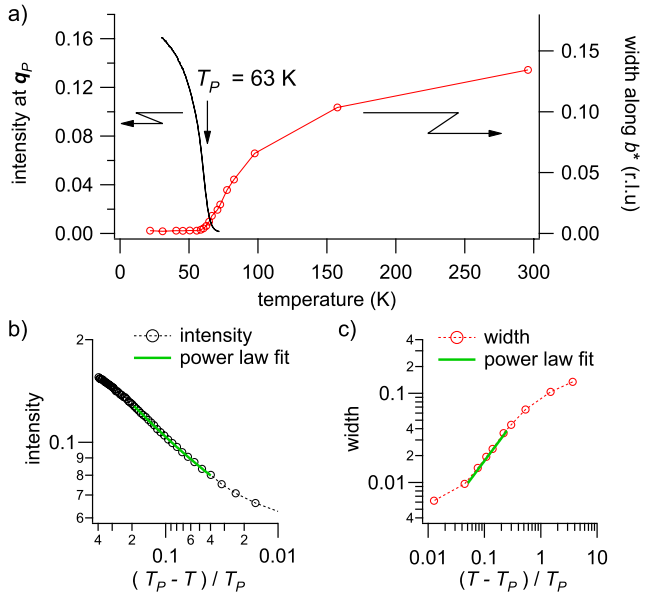

FIG. 4 (color online). (a) Temperature dependence of superstructure intensity at — (left scale) and the width of the diffuse scattering along $b*$ (right scale). (b),(c) Double-logarithmic representations of the intensity and the width, respectively, versus the reduced temperature.

not be derived; in particular, the shape of the diffuse scattering peak along a^* and c^* is not accessible due to its large width on a sloping strong background.

The critical exponent $\beta = 0.13 \pm 0.03$ is even smaller than the ones observed in other CDW materials [0.32 ± 0.05 for blue bronze [9] and 0.23 ± 0.02 for $(TaSe_4)_2I$ [10]]. Thus, a mean field description of the phase transition is not appropriate and fluctuation corrections are needed. Such small exponents β of the order parameter are best compatible with a two-dimensional order parameter. The diffuse scattering spot is well defined in momentum space, and the Kohn anomaly is sharp in three dimensions; thus, above T_P a three-dimensional fluctuation regime is observed. Furthermore, the exponent ν of the correlation length is compatible with a three-dimensional XY universality class [18]. On the other hand, the Peierls transition could be considered as a discontinuous freezing (first order) that is blurred by the presence of defects and thus rendered continuous. This would also lead to a power law with a small exponent [10]. However, our experiment did not show any hysteresis in temperature scans, and only a slight specific heat anomaly was reported in $ZrTe_3$ [16]. Thus, we conjecture that the phase transition is continuous (second order) or very close to that.

In summary, we have identified the soft phonon mode that stabilizes the charge density modulation in $ZrTe_3$ and measured its temperature dependence. It is an acoustic a^* polarized phonon branch with a mostly transverse dispersion along c^*. The Kohn anomaly is observed already at high temperatures of 3–4 T_P and only for a sharp momentum space region around $\vec{q}_P$. On approaching the phase transition, it becomes giant and the phonon freezes into a static modulation of the lattice. The temperature dependence of the softening does not follow mean field predictions. The analysis of superstructure diffraction intensity and diffuse scattering correlation lengths lead to the conclusion that the phase transition is continuous but governed by an order parameter of dimension $n = 2$.

We thank D. Gambetti and P. Dideron for technical assistance. Fruitful discussion with R. Currat, P. Monceau, S. V. Maleyev, and J.-P. Pouget are gratefully acknowledged. We also thank Swiss-Norwegian beam lines at ESRF for the beam-time allocation necessary for preliminary mapping of reciprocal space. This work was performed at the European Synchrotron Radiation Facility.

[1] G. Grüner, *Density Waves in Solids*, Frontiers in Physics Vol. 89 (Perseus Publishing, Cambridge, MA, 1994).
[2] S. Kivelson and V. Emery, Synth. Met. **80**, 151 (1996).
[3] P. Lee, T. Rice, and P. Anderson, Phys. Rev. Lett. **31**, 462 (1973).
[4] B. Renker, H. Rietschel, L. Pintschovius, W. Gläser, P. Brüesch, D. Kuse, and M. J. Rice, Phys. Rev. Lett. **30**, 1144 (1973).
[5] J. P. Pouget, B. Hennion, C. Escribe-Filippini, and M. Sato, Phys. Rev. B **43**, 8421 (1991).
[6] H. Fujishita, S. M. Shapiro, M. Sato, and S. Hoshino, J. Phys. C **19**, 3049 (1986).
[7] J. E. Lorenzo, R. Currat, P. Monceau, B. Hennion, H. Berger, and F. Levy, J. Phys. Condens. Matter **10**, 5039 (1998).
[8] H. Requardt, J. E. Lorenzo, P. Monceau, R. Currat, and M. Krisch, Phys. Rev. B **66**, 214303 (2002).
[9] S. Girault, A. H. Moudden, and J. P. Pouget, Phys. Rev. B **39**, 4430 (1989).
[10] H. Requardt, M. Kalning, B. Burandt, W. Press, and R. Currat, J. Phys. Condens. Matter **8**, 2327 (1996).
[11] D. J. Eaglesham, J. W. Steeds, and J. A. Wilson, J. Phys. C **17**, L697 (1984).
[12] S. Takahashi, T. Sambongi, and S. Okada, J. Phys. (Paris), Colloq. **44**, C3-1733 (1983).
[13] C. Felser, E. Finckh, H. Kleinke, and W. Tremel, J. Mater. Chem. **8**, 1787 (1998).
[14] K. Stöwe and F. Wagner, J. Solid State Chem. **138**, 160 (1998).
[15] T. Yokoya, T. Kiss, A. Chainani, S. Shin, and K. Yamaya, Phys. Rev. B **71**, 140504(R) (2005).
[16] M. Chung, Y. Wang, and J. W. Brill, Synth. Met. **56**, 2755 (1993).
[17] A. Zwick, M. Renucci, and A. Kjekshus, J. Phys. C **13**, 5603 (1980).
[18] G. A. Baker, B. G. Nickel, and D. I. Meiron, Phys. Rev. B **17**, 1365 (1978).